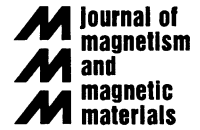




ELSEVIER

Journal of Magnetism and Magnetic Materials 225 (2001) 277–284



www.elsevier.com/locate/jmmm

Progenitor cell isolation with a high-capacity quadrupole magnetic flow sorter

Lee R. Moore^a, Alexander R. Rodriguez^a, P. Stephen Williams^a,
Kara McCloskey^b, Brian J. Bolwell^a, Masayuki Nakamura^b,
Jeffrey J. Chalmers^b, Maciej Zborowski^{a,*}

^aDepartment of Biomedical Engineering/ND20, and Bone Marrow Transplantation Program, The Cleveland Clinic Foundation, 9500 Euclid Avenue, Cleveland OH 44195, USA

^b121 Koffolt Laboratories, Department of Chemical Engineering, The Ohio State University, 140 West 19th Avenue, Columbus OH 43210-1180, USA

Abstract

Rapid and efficient sorting is important for progenitor cell isolation. Therefore, we have built and evaluated a high-speed, continuous flow, quadrupole magnetic sorter. The cross-over behavior of non-magnetic particles, combined with separation theory is used to optimize performance. CD34 + progenitor cells are separated to purities from 64–95% and a throughput of 10^7 cells/s. © 2001 Elsevier Science B.V. All rights reserved.

Keywords: Magnetic cell separation; Immunomagnetic separation; Cell sorting; Quadrupole separator; Magnetic particle; Progenitor cell; CD34 +

1. Introduction

The separation of heterogeneous cell populations based on the expression of a surface marker has significant preparative applications in biology and medicine. The available immuno-separation methods and their ligands include fluorescence-activated cell sorting (FACS) requiring fluorescent labels conjugated to antibodies, immunoaffinity columns requiring antibodies immobilized to solid-phase supports, and magnetic separation requiring antibodies attached to magnetic nanospheres or microspheres [1–3]. Of these, FACS is the most

widely used, and is applied to cell analysis and sorting. Automated FACS sorters are capable of sorting to high purities and recoveries. Fluorochromes with different emission wavelengths can be used concurrently, allowing for multi-parameter separations. The disadvantages of FACS are the low viability of recovered cells, the high cost and difficulty of use of the complex equipment, and relatively low throughput (typically, on the order of 10^3 cells/s).

Continuous immunomagnetic cell sorting, as realized by our quadrupole magnetic flow sorter (QMS), offers a comparatively simple and inexpensive device, gentle handling and high viability of the sorted fractions, and high throughput (on the order of 10^7 cells/s). A disadvantage is that cell selection is limited to a single parameter, cell magnetization.

*Corresponding author. Tel.: +216-445-9330; fax: +216-444-9198.

E-mail address: zborow@bme.ri.ccf.org (M. Zborowski).

Another limitation, common to any dynamic process, is that prior knowledge of the separand properties is required to optimize the performance.

Numerous commercial magnetic labels are available, ranging from micrometer- to nanometer-sized. We have chosen antibody–magnetic nanosphere conjugates because the small size of the beads permits a linear relationship between cell marker number and magnetization [4,5]. The comparatively low cell magnetic moment is compensated by a magnet design with a high field and gradient, as described below.

2. Materials and Methods

2.1. Apparatus

Fig. 1 presents the flow cell and magnet of the large-scale QMS. This device differs from another reported earlier in that the length and aperture of the magnet are larger, while the maximum field at the poles, B_0 , is significantly greater [6,7]. The magnet structure is built by Dexter Magnetics Corp., Toledo, OH, according to designs provided by us. The magnet has a bore radius of 8.0 mm and the bore is 155 mm long. The field is provided by four neodymium–iron–boron permanent magnets. An average B_0 is determined from measurements of B at the pole tips versus z over the length of the magnet, using a Gauss meter and Hall-effect probe (Model 9200 Gaussmeter and transverse probe STG920404, F.W. Bell, Orlando, FL) (data not shown). Significant edge effects are not detected at z -distances inside the magnet greater than about 5 mm. The average B_0 is 1.42 T.

The flow cell consists of a concentric outer cylinder, a solid inner rod, and short cylinders at the entrance and exit, which function as flow splitters. The splitters separate the entering feed and carrier flow components, designated as a' and b' , as well as depleted and enriched flow components, a and b . The magnetic force acts in the annular space between the splitters, and the annular thickness of the Mark Vb channel used in these experiments is 902 μm . The schematic of Fig. 2 presents the entire experimental set-up. The component flows, $Q_{a'}$, $Q_{b'}$, Q_a and Q_b are controlled by two Harvard

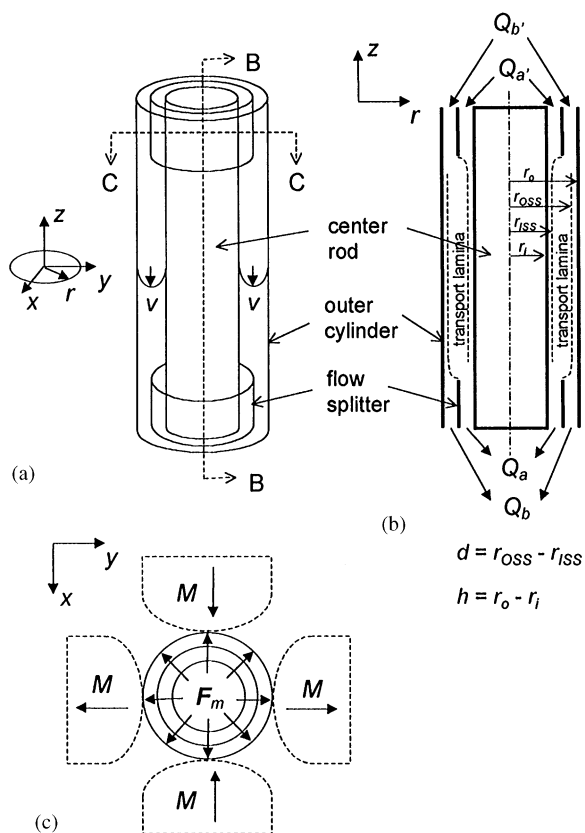


Fig. 1. Schematic of the quadrupole magnetic flow sorter (QMS) separation element. A. Perspective view of the flow channel showing fluid velocity profile in the annulus. B. Longitudinal section of flow channel as shown in A. Note positions of the inlet splitting surface (ISS) and the outlet splitting surface (OSS). C. Cross-section through magnetic poles and flow channel, as indicated in A, showing radial magnetic force, F_m .

'33' dual syringe pumps (Harvard Instruments, Inc., Holliston, MA). A six-way valve with a 500- μl loop (Rheodyne 7725i, Alltech Associates, Inc., Deerfield, IL) is used for pulse-injection of the cell samples. The valve could be set to 'load' enabling the loop to be filled. In this position the loop is bypassed with a short circuit between the buffer-containing feed syringe and the flow channel. When the valve is switched to 'inject', the loop is restored back into the circuit allowing its contents to be injected into the channel. The outlets, a and b , from the flow channel are connected to two 254-nm UV detectors with 32 μl flow cells (VUV-10,

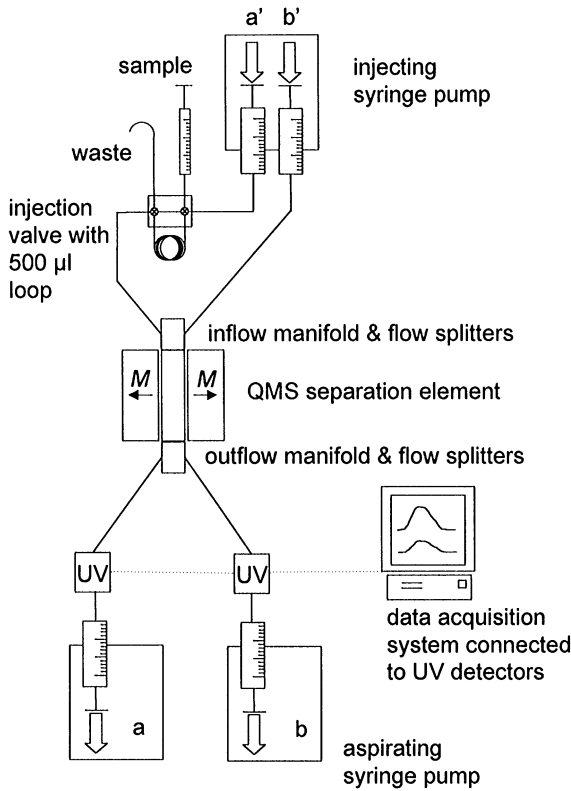


Fig. 2. Block diagram of QMS system.

HyperQuan, Inc., Colorado Springs, CO). The analog signal from the detectors is fed to a two-channel analog-to-digital converter (DI-190, Dataq Instruments, Akron, OH). The digital data is presented, stored and subsequently analyzed on a PC (software package WinDaq Lite, Dataq Instruments). Elution peaks are processed and integrated with additional software (PeakFit, SPSS, Inc., Chicago, IL).

2.2. Cell tracking velocimetry

The magnetic mobilities of a population of cells can be measured by an apparatus and technique known as cell tracking velocimetry (CTV) [8–12]. A microscope, CCD camera and VCR record the motions of magnetically labeled cells in a narrow glass channel placed in a magnet structure which provides a constant S_m , as defined by Eq. (2), below. The video playback is acquired to PC by image-

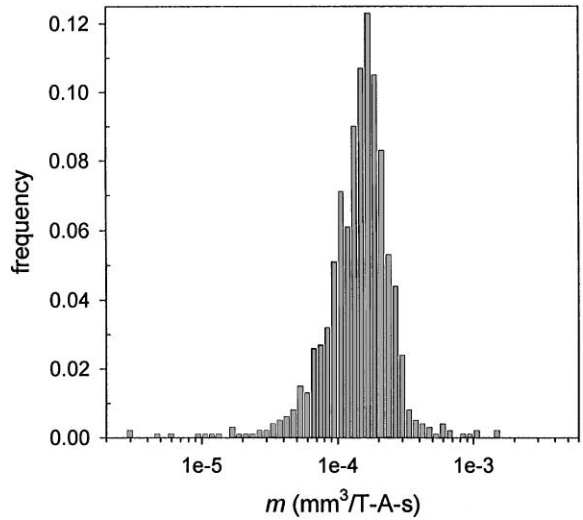


Fig. 3. Mobility histogram of immunomagnetically-labeled CD34 + cells obtained from cell tracking velocimetry (CTV).

grabbing software and digitized so that each pixel is assigned a binary number. C++ code compares the successive frames to compute velocities for multiple particles tracked in the channel. With Eq. (1), the velocities are converted to mobilities. These steps are repeated until hundreds to thousands of cells or particles are processed. Presentation of frequency versus mobility data gives rise to histograms, as in Fig. 3.

2.3. Theory of separation

Thorough descriptions of the fluid dynamic and magnetic theory applicable to the QMS are given elsewhere [13–15]; the following is a summarized account. Magnetically labeled cells in a magnetic field experience a magnetic drift velocity, u_m :

$$u_m = mS_m, \tag{1}$$

where m is the cell magnetophoretic mobility and S_m is the field strength parameter. In the general case, S_m is described for a particle of inducible magnetization, such as a paramagnetic nanosphere, as

$$S_m = \frac{|\nabla B^2|}{2\mu_0}, \tag{2}$$

where μ_0 is the permeability of free space. In the ideal quadrupole system, it can be shown that S_m is related to the system parameters by

$$S_m = \frac{B_0^2}{\mu_0 r_0} \frac{r}{r_0}. \quad (3)$$

B_0 , in this case, is the flux density at the inner surface of the outer cylinder, r_0 (see Fig. 1) and r is the radial coordinate originating at the axis. Note that there is no dependence on the angular coordinate, θ . The magnetophoretic mobility is independent of the magnetic environment and relates to properties of the cell, label and medium by

$$m = \frac{2}{9} \frac{R^2 \Delta\chi}{\eta}, \quad (4)$$

where R is the cell radius, η is the medium viscosity and $\Delta\chi$ is the difference between the volumetric susceptibilities of the cell and the medium. Comparing the above equations, it is apparent that the velocity increases linearly as a cell moves from the rod surface at r_i toward the outer cylinder.

The fluid velocity profile in the annulus between the splitters is roughly parabolic and approaches ideal parabolic behavior as the annular width, $r_0 - r_i$, approaches zero. The component flows converge just beyond the inlet splitter, and the virtual boundary separating the fluids and extending down the column, is called the inlet splitting surface (ISS); see Fig. 1. The radial position of the ISS depends non-linearly on the ratio of the feed component flow to the total flow, Q_a/Q :

$$\frac{Q_a}{Q} = \frac{[2\rho^2 - \rho^4 + 2A_2\rho^2 \ln \rho - A_2\rho^2]_{\rho_i}^{\rho_{\text{ISS}}}}{A_1(1 - \rho_i^2)}, \quad (5)$$

where A_1 and A_2 are constants which depend on the channel geometry and ρ is the ratio r/r_0 . A similar outlet splitting surface (OSS) extends upward from the outlet splitter and separates the flow components a and b . Analogous to Eq. (5), the position of the OSS depends on Q_a/Q . The transport lamina thickness, d , is the distance between the splitting surfaces. Conceptually, the transport lamina may be thought of as a virtual filter whose ability to reject cell passage through it increases with d .

2.4. Flow rate optimization

Substitution of Eqs. (3) and (4) into Eq. (1) gives the radial velocity component for a cell of known mobility. If the sedimentation rate is assumed to be relatively small, the cell axial velocity component is just the axial fluid velocity at the local radial position. The combination of these velocity components gives cell trajectories:

$$z = \frac{Q}{2\pi A_1 r_0 S_{m0} m (1 - \rho_i^2)} \times [4 \ln \rho - 2\rho^2 + 2A_2(\ln \rho)^2]_{\rho_i}^{\rho}, \quad (6)$$

where S_{m0} is just S_m at $r = r_0$, and z is the distance along the channel axis. Eq. (6) combined with prediction of ISS and OSS positions from flow rate components enable recoveries to be determined for a selected flow rate, Q , and for a population of labeled cells whose mobilities have been determined by CTV. These calculations have been committed to computer code (Maple V Release 4, Waterloo Maple, Inc., Ont., Canada).

2.5. Cell labeling

The source of hematopoietic progenitor cells for the QMS experiments is a small sample of the white blood cell fraction from patients undergoing clinical apheresis for subsequent autologous donation for cancer therapy. Prior to apheresis collection the patients underwent progenitor cell mobilization by exposure to chemotherapeutic agents and growth factors, in order to increase circulating progenitor cell concentration. The use of the patient samples for this study is approved by the Institutional Review Board, and it required signed consent by the patients.

A 10-ml apheresis sample containing at least 10^9 mononuclear cells is washed with a buffer containing 0.5% bovine serum albumin (BSA) and 2 mM EDTA in Ca- and Mg-free phosphate-buffered saline (BSA). Subsequent to treatment with hypotonic medium to lyse the red cells, the concentration of the cell suspension is determined by a Coulter Z-1 particle counter (Beckman-Coulter, Fullerton, CA). Three hundred million cells, a sufficient

number to perform a group of three experiments, are removed for labeling. A complex of differentiation number 34 (CD34) is used as the distinguishing cell surface molecule for blood progenitor cells. The cells are labeled with FcR blocking reagent, anti-CD34 (QBEND/10 epitope) hapten conjugate, and anti-hapten magnetic nanospheres (MACS CD34 Progenitor Cell Isolation kit, Miltenyi Biotec, Auburn, CA). In order to assess the purity and recovery of the separation with flow cytometry, the progenitor cells are then targeted with anti-CD34-(HPCA-2 epitope)-FITC. The cells are washed after each labeling step and finally reconstituted to 2.0 ml with buffer, yielding a concentration of about 10^8 cells/ml, as determined with the particle counter. A 10- μ l sample is removed for flow cytometry analysis of the CD34 + feed purity; the remaining volume is sufficient for three experiments of 500- μ l injections.

2.6. Experimental procedure

The pulse-injection technique employed in cross-over studies has been described thoroughly [16]. The flow channel is prefilled with degassed buffer, with particular attention paid to removal of air bubbles. Syringes of volumes 30, 140, 60 and 140 cm^3 are used with tubings to a' , b' , a and b . The inlet syringes are pre-filled with buffer, and then all are attached to the syringe pumps. Both pumps are started at once, while the detector trace is monitored. In the meantime, the sample loop is slightly overfilled to ensure uniform concentration, by injecting 600 μ l from a syringe. When the detector baseline signals are steady, the injection valve is moved from 'load' to 'inject' position, as absorbance data is stored on the PC hard disk. When the detector signals return to the baseline, it is assumed that the entire sample has eluted from the column, so the pumps and data acquisition are stopped.

The following additional steps are taken in cell separation experiments. Syringes a and b are weighed before and after sample injection to determine the volumes collected, while the cell concentrations in these syringes are determined with the particle counter. Samples from both outlets are fixed with para-formaldehyde for sub-

sequent flow cytometry determination of CD 34 cell purity. The process is repeated twice for each apheresis sample.

3. Results

3.1. Channel evaluation

For the isolation of rare cells, the non-specific cross-over of a few negative cells beyond the OSS can have a severely adverse effect on the purity of the enriched fraction, b . For this reason, and to compare the performance of prototype channels of differing geometries, a method is devised to evaluate cross-over. Cross-over is believed to be caused by hydrodynamic effects or possible geometric imperfections in the flow channel.

Monodisperse 7.6- μ m polymeric spheres are used to emulate unlabeled cells. 500- μ l samples of particle suspension are pulse-injected into the Mark Vb channel and analyzed with a method described elsewhere [16]. In one set of experiments, the inlet flow rate ratio, Q_a/Q , and the total flow rate, Q , are maintained at 0.2 and 10 ml/min. In this case, the ISS remained at 262.5 μ m from the inner rod — or $0.291h$ where h is the annular thickness — and 638.2 μ m from the outer cylinder. Starting with an outlet flow rate ratio, Q_a/Q , of 0.2 and increasing this ratio in small steps results in a transport lamina thickness, d , increasing from 0 (see Fig. 4). The recovery in b , F_b , drops steadily with increasing d with most of the decrease occurring between 0 and 55.9 μ m (Q_a/Q ranging from 0.20 to 0.28). The recovery in a , F_a , is such that the sum of F_a and F_b is consistently between 0.8 and 0.9 indicating some systematic losses.

The practical application is that these studies enable one to predict a flow rate satisfying a maximum cross-over limit, such as 1% or less. Or, for a given purity in the cell feed and flow rate ratios, we can estimate the maximum purity obtainable in the enriched fraction b . For example, with a feed purity of 1.0% and a cross-over of 1.0%, the maximum purity attainable when all the positive cells are recovered in b is $1.0/(1.0 + 0.99) = 50.3\%$.

To investigate the effect of the total flow rate on cross-over, a separate set of experiments is

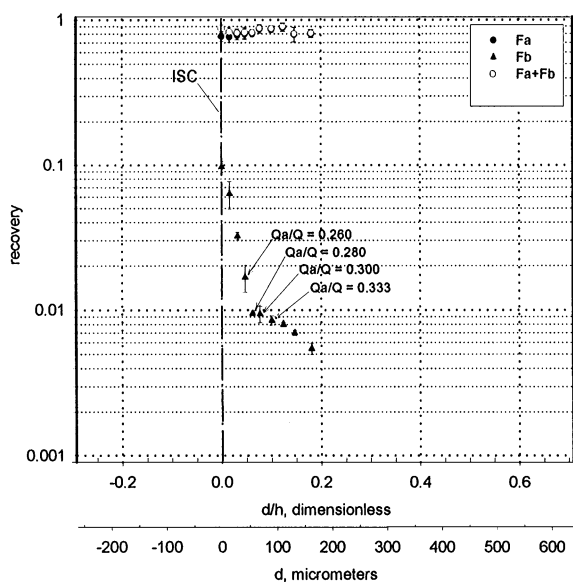


Fig. 4. Cross-over of 7.6 μm polystyrene beads in Mark Vb QMS channel. The annular boundaries — the core rod surface and inner surface of the outer cylinder — are shown in heavy lines, left and right. The inner splitting surface (ISS) separating inlet a' and b' flows, is marked. The triangular points denote recovery in b , F_b , corresponding to variable outer splitting surface (OSS) positions, which, in turn, are governed by various outlet flow rate ratios, Q_a/Q . The recovery in a , F_a and $F_a + F_b$, are shown as circles.

performed where Q is varied from 5 to 40 ml/min and Q_a'/Q and Q_a/Q are fixed at 0.1 and 0.125, yielding a transport lamina of $d = 23.1 \mu\text{m}$ (see Fig. 5). As in the previous case, about 10% of the particles are not recovered in a or b when the total flow rate is $Q = 10 \text{ ml/min}$. At $Q = 5 \text{ ml/min}$, losses exceed 40%, strongly suggesting that sedimentation is to blame. The cross-over drops steadily until Q is about 30 ml/min where it remains stationary between 3% and 5%. The decrease in cross-over at higher Q is fortuitous as practical considerations require that Q should be 30 ml/min or higher.

A transport lamina of this thickness occurs in the previous experiment where Q_a'/Q is 0.2, when Q_a/Q lies between 0.22 ($d = 14.6 \mu\text{m}$) and 0.24 ($d = 28.7$). Interpolating, we would expect a cross-over of 4.5%, much lower than the 25.7% we see in Fig. 5 when $Q = 10 \text{ ml/min}$. This suggests that

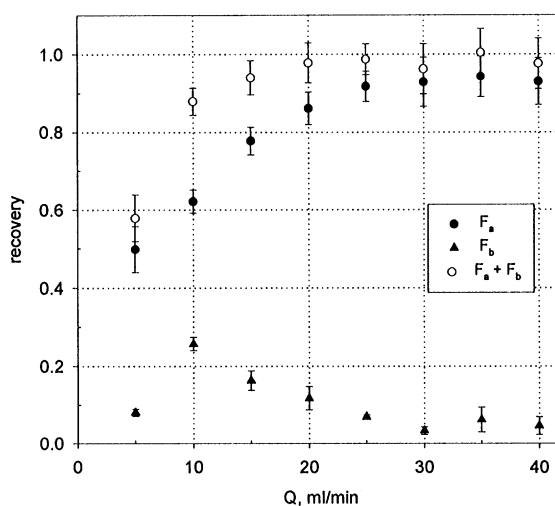


Fig. 5. Cross-over of 7.6- μm polystyrene beads in Mark Vb QMS channel as a function of fixed flow rate ratios and variable total flow rate. Q_a'/Q is 0.1 and Q_a/Q is 0.125 giving rise to a transport lamina thickness of 23.1 μm .

cross-over is greater when d and Q are matched and Q_a'/Q is reduced.

3.2. Cell sorting experiments

Two groups of experiments are performed. In the first group, A, all conditions are identical, and the three repetitions evaluate the reproducibility of the method. In the second group, B, the flow components were changed to investigate the effects of transport lamina thickness on cross-over. Table 1 summarizes the results. In Group A the feed purity in CD34 cells is increased from 1.4% to a range from 89.8% to 95.3% (Fig. 6). Recovery in b ranged from 26.5% to 30.9%, while the total recovery of positive cells exceeded 90%. The large increases in purity over the feed gives rise to a large enrichment rate in b . Flow rates and feed concentrations are chosen to give a throughput of about 10^7 cells/s, resulting in a theoretical separation time of 5 s. With additional time allowed for the detectors to stabilize before injection as well as time to ensure that all the cells are eluted, the total processing time is about 1 min.

The inlet flow rate ratio results in an ISS, as shown in Fig. 4; the OSS corresponding to $Q_a/Q = 0.333$ gives a cross-over of 0.85%. With

Table 1
Separation results of CD34⁺ progenitor cells obtained from apheresis product

Experiment group and number	A			B		
	1	2	3	1	2	3
Feed total cell concentration $\times 10^{-8}$ (cells/ml)		1.22			0.929	
Feed purity ^a (%)		1.4			8.1	
Flow rate (ml/min)						
<i>a'</i>		6			6	
<i>b'</i>		24			24	
<i>a</i>		10		8	9	10
<i>b</i>		20		22	21	20
Transport lamina thickness, <i>d</i> (μ m)		90.6		47.0	69.1	90.6
Purity (%)						
<i>a</i>	0.89	0.95	0.92	4.9	4.7	8.2
<i>b</i>	89.8	95.3	94.9	63.9	70.1	89.1
Recovery ^b (%)						
<i>a</i>	62.6	64.7	66.5	42.4	41.4	69.3
<i>b</i>	30.9	27.0	26.5	43.7	35.6	31.2
Enrichment rate	656	1512	1387	23.9	31.6	109.9
Throughput $\times 10^{-7}$ (cells/s)		1.22			0.93	
Theoretical recovery (%)						
<i>a</i>		24.8		13.1	18.5	24.8
<i>b</i>		73.0		84.7	79.3	73.0

^aPurity is defined as the fraction of the CD34⁺ cells in the sample.

^bRecovery is defined as the fraction of the CD34⁺ cells in the feed sample which was recovered in the sorted fraction.

a feed purity of 1.36% the maximum purity in *b* should be $1.36/(1.36 + (100 - 1.36)0.0085) = 61.9\%$. The cross-over data were acquired at $Q = 10$ ml/min, while the cell experiments were performed at $Q = 30$ ml/min, so the cross-over for the cell studies should be lower than predicted in Fig. 4, if we consider the trend of decreasing cross-over at higher flow rates shown in Fig. 5. Also, deformable cells might have a different cross-over mechanism than rigid polymeric spheres.

Except for the slight differences in outlet flow rates, the experiments of B are performed under conditions similar to those of Group A. Since the apheresis samples had their origins in different patients — as seen by the big difference in feed purities — a strict comparison between the groups is not possible. CTV analysis was not available for these experiments, so we cannot assume that they had similar mobility distributions, or that either mobility distribution resembled that of Fig. 3. Nonetheless, for the sake of comparison, the theoretical

recoveries for cell mobilities presented in Fig. 3 are listed in Table 1. The lower-than-expected actual recoveries in Groups A and B might be due to sample mean mobilities significantly different than the 1.5×10^{-4} value used in the theoretical computation.

The purities followed the expected trend of increasing with increasing *d*. Likewise, increasing *d* had the expected effect of rejecting more cells from the OSS and decreasing the recoveries in *b*. This effect of transport lamina thickness on recovery and purity has been previously reported [6,7]. Higher purities result in higher enrichment rates, although the high feed purity limited the enrichment rate in B compared to A. Using the same approach used in Group A, the maximum theoretical purities in *b* should be 86.7%, 90.3% and 91.1% for experiments 1–3. This time, these are not exceeded by the results.

Previous work demonstrates good agreement between theoretical and experimental recoveries [16].

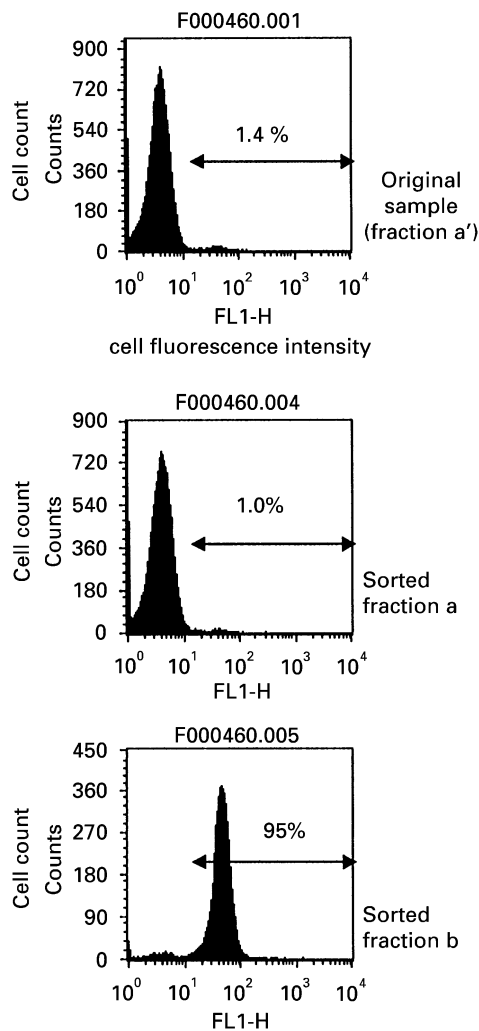


Fig. 6. Illustrative flow cytometry histograms of CD34 + cells sorted in the QMS. The arrows delineate the range of fluorescence intensities of CD34 + cells.

Disparities listed in Table 1 are due to the fact that the mobility is obtained from a sample different from those of the experiments. Differences between patient samples indicate the need for CTV analysis of mobilities on each sample, a practice we are in the process of implementing. Further, agreement between actual and predicted purities is weak because of poorly understood cellular interactions, and because the conditions of the cross-over experiments do not strictly coincide with those of the cell separation experiments. We are addressing the

former with additional steps to process and characterize the feed. New cross-over studies are planned to better match cell separation conditions.

Acknowledgements

This study was supported by grants from the NIH (R01 CA62349 to M.Z., R33 CA81662 to J.J.C.; and R43 CA83466, as a subcontract from Biomec Inc., Cleveland, OH) and from the NSF (BES-9731059 to J.J.C. and M.Z.). Technical assistance of Mr. Boris Kligman is thankfully acknowledged.

References

- [1] H.M. Shapiro, *Practical Flow Cytometry*, Wiley-Liss, New York, 1995.
- [2] K. Auditore-Hargreaves, S. Heimfeld, R.J. Berenson, *Bioconjugate Chem.* 5 (1994) 287.
- [3] S. Miltenyi, W. Müller, W. Weichel, A. Radbruch, *Cytometry* 11 (1990) 231.
- [4] J.J. Chalmers, M. Zborowski, S. Mandal, B. Fang, L. Sun, *Biotechnol. Bioeng.* 59 (1998) 10.
- [5] K.E. McCloskey, J.J. Chalmers, M. Zborowski, *Cytometry* 40 (2000) 307.
- [6] M. Zborowski, L. Sun, L.R. Moore, J.J. Chalmers, *ASAIO J.* 45 (1999) 127.
- [7] L. Sun, M. Zborowski, L.R. Moore, J.J. Chalmers, *Cytometry* 33 (1998) 469.
- [8] M. Nakamura, J.J. Chalmers, L. Lasky, M. Zborowski, *Exp. Fluids* 2000, in press.
- [9] L.R. Moore, M. Zborowski, M. Nakamura et al., *J. Biochem. Biophys. Methods* 44 (2000) 115.
- [10] J.J. Chalmers, S. Haam, Y. Zhao et al., *Biotechnol. Bioeng.* 64 (1999) 509.
- [11] J.J. Chalmers, S. Haam, Y. Zhao et al., *Biotechnol. Bioeng.* 64 (1999) 519.
- [12] J.J. Chalmers, Y. Zhao, M. Nakamura et al., *J. Magn. Magn. Mater.* 194 (1999) 231.
- [13] P.S. Williams, M. Zborowski, J.J. Chalmers, *Anal. Chem.* 71 (1999) 3799.
- [14] M. Zborowski, in: U. Häfeli, W. Schütt, J. Teller, M. Zborowski (Eds.), *Scientific and Clinical Applications of Magnetic Microcarriers: An Overview*, Plenum Press, New York, 1997, p. 205.
- [15] M. Zborowski, P.S. Williams, L. Sun et al., *J. Liquid Chromatogr. Relat. Tech.* 20 (1997) 2887.
- [16] M. Hoyos, L.R. Moore, K.E. McCloskey et al., *J. Chromatogr. A* 903 (2000).